sustainability

MDPI

Article

Hybrid Microgrid Sizing Using Particle Swarm Optimization with Use-Case Objective Functions: A Resilience-Focused Approach

Andrea Micangeli [1,*], Alessio Azadi [1], Massimo Schiavetti [2], Marco Balsi [3], Soufyane Bouchelaghem [3] and Semereab Habtetsion [4]

[1] DIMA, Department of Mechanical and Aerospace Engineering, Sapienza University of Rome, 00184 Rome, Italy; azadigrid@gmail.com
[2] Independent Researcher, Via Andrea Pisano, 56122 Pisa, Italy; massimo.schiavetti1@gmail.com
[3] Department of Information Engineering, Electronics and Telecommunications, Sapienza University of Rome, 00184 Rome, Italy; marco.balsi@uniroma1.it (M.B.); soufyane.bouchelaghem@uniroma1.it (S.B.)
[4] Independent Researcher, Denden Street, Asmara P.O. Box 5716, Maekel Region, Eritrea; semereabhh@gmail.com
* Correspondence: andrea.micangeli@uniroma1.it

Abstract

While traditional microgrid optimization focuses primarily on minimizing Net Present Cost (NPC), real-world deployment success depends on multiple operational factors, including system resilience, capacity headroom, and battery health preservation. This paper presents an enhanced Particle Swarm Optimization (PSO) framework coupled with a Multi-Design Optimization (MDO) methodology that incorporates use-case objective functions that take into account several metrics beyond pure economics. Moreover, the enhanced PSO algorithm allowed us to evaluate near-optimal solutions that can help with plant design with constrained industrial choices. The proposed approach extends the established PSO-MDO method by introducing a customized cost function that simultaneously evaluates: (i) economic viability through NPC, (ii) system resilience through capacity factor and headroom utilization, and (iii) battery longevity through Depth of Discharge (DoD) and C-rate constraints. We apply this methodology to the Areza microgrid in Eritrea, a remote PV-BESS-diesel hybrid system that has been operational since 2019, with two primary objectives: first, quantifying design differences between optimization-derived and as-built configurations, and second, assessing system resilience under load growth scenarios. The results demonstrate that the objective function reveals critical trade-offs invisible to traditional NPC-only optimization, particularly regarding battery stress patterns and system capacity margins. The results reveal a broad near-optimal range where NPC changes by about 5%, but CAPEX varies by almost 28%. This indicates how very different combinations of components can achieve similar lifecycle costs. The best-performing design achieves an NPC ≈ EUR 2.02 M and an LCOE ≈ EUR 0.161/kWh, with sizing around PV 973 kW, battery 2236 kWh, inverter 392 kW, and generator 522 kW. The study highlights key trade-offs: reducing diesel use often leads to more curtailment, and systems that rely more on diesel are more sensitive to demand growth. Smaller systems face higher fuel costs when demand rises by 20%.

Keywords: microgrid optimization; Particle Swarm Optimization; Multi-Design Optimization; battery energy storage systems; resilience analysis; rural electrification; use-case cost function

Check for updates

Academic Editor: Babatunde Olubayo

Received: 28 May 2026
Revised: 22 June 2026
Accepted: 1 July 2026
Published: 16 July 2026

1. Introduction

1.1. Context and Motivation

Rural electrification through hybrid microgrids represents a critical pathway for sustainable development in off-grid communities [1,2]. Although significant progress has been made in developing optimization tools for microgrid design, a persistent gap exists between theoretically optimal designs and practically deployable systems, matching available components, and single use-case specificity. Traditional sizing methodologies predominantly focus on minimizing Net Present Cost (NPC), potentially overlooking critical operational factors such as system resilience, battery health, productive use of electricity, and capacity to accommodate future load growth.

This work directly contributes to Sustainable Development Goal 7 (SDG 7): ensuring access to affordable, reliable, sustainable, and modern energy for all. Off-grid hybrid microgrids combining solar PV with battery storage represent a key technology pathway for achieving universal electrification targets, particularly in sub-Saharan Africa, where over 565 million people remained without electricity access in 2023 [1]. By explicitly incorporating resilience and battery health metrics into the optimization framework, the proposed methodology promotes systems that are not only economically viable but also operationally sustainable over their full project lifetime, reducing the risk of stranded assets in remote communities.

In stationary microgrid systems, batteries are now more widely used than other lithium-ion types. This shift is not driven by energy density, where LFP remains inferior, but by characteristics that are particularly relevant in remote and rural environments. LFP batteries handle high temperatures well, are less likely to overheat, and last longer with frequent use. These qualities make them a strong choice for locations that require minimal supervision or can withstand harsh weather. As a result, developers can build microgrids that rely on batteries for power and backup, rather than relying primarily on diesel generators [3,4].

This study is the first application of the modified PSO-MDO framework to the analysis of the near-optimal neighborhood of a real microgrid. Its primary contribution is methodological: showing that the use-case-oriented post-processing of the near-optimal region can surface resilience, headroom and battery-health trade-offs that least-cost ranking hides, using the Areza system and its SCADA data as a testbed. Accordingly, several analyses are deliberately scoped as a foundation for subsequent work: the exhaustive breaking-point quantification across all candidate designs, the sizing of recovery capacity, multi-run convergence statistics, and economic and data-treatment sensitivity studies. We report directional findings where the available data support them and identify, in each case, the next step required to make them exhaustive.

1.2. Research Gap and Innovation

Recent advances in heuristic optimization methods, particularly the Multi-Design Optimization (MDO) framework proposed by [5,6], have demonstrated that multiple significantly different design configurations can yield similar NPC values within narrow tolerance bands (1–5%). This finding suggests that the objective function landscape is relatively flat near the optimum, opening opportunities for incorporating additional criteria without substantially compromising economic efficiency.

However, existing MDO implementations continue to rely on NPC as the sole optimization criterion during the iterative search process, with additional metrics examined only during post-processing. This approach limits the algorithm's ability to actively guide the search toward solutions that balance multiple objectives throughout the optimization process.

https://doi.org/10.3390/su18147263

An example of objective metrics that should be considered in the design evaluation follows:

- Economic metrics: NPC, LCOE, and initial CAPEX;
- Resilience indicators: Capacity factor achieved, system headroom utilization;
- Battery health preservation: Average and maximum DoD, C-rate distribution;
- Operational flexibility: Unmet energy, curtailed generation, protection mode frequency.

This work addresses this limitation not by altering the PSO objective itself, which remains a single-objective Net Present Cost (NPC) minimization, but by introducing a use-case-oriented post-processing stage. After optimization, the near-optimal region around the cost minimum is analyzed against additional, deployment-relevant criteria (resilience, capacity headroom, depth-of-discharge and C-rate stress), allowing multiple design options to be compared on dimensions that pure cost ranking does not capture.

1.3. Case Study: The Areza Microgrid

Areza is a rural town in Eritrea's Debub Administrative Region (Zoba Debub), 42 km west of Mendefera, the capital of Zoba Debub, latitude 14.92575° and longitude 38.56503° at an elevation of 2008 m (6588 feet). Figure 1 illustrates the geographic position of the site within the Horn of Africa. The Areza microgrid has been operational since 2019; it provides an ideal testbed for this methodology.

Figure 1. Location of the Areza microgrid site in Eritrea (red arrow), with an inset map showing the regional context in the Horn of Africa. Red rectangle indicates position of the inset within the region.

1.4. Research Objectives

This study pursues two primary objectives:

- Objective 1: Design Comparison. Quantify the differences between PSO-optimized microgrid configurations and the actual deployed Areza system, analyzing trade-offs in component sizing, economic performance, and operational characteristics.

- Objective 2: Preliminary Resilience Characterization. Demonstrate that the near-optimal post-processing can track resilience indicators (energy adequacy, battery depth-of-discharge and C-rate stress) under progressive load growth, reporting directional trends and the first binding constraint, and establishing the basis for an exhaustive per-design breaking-point and recovery-capacity analysis in future work. Through these objectives, we demonstrate the practical utility of use-case-oriented post-processing of near-optimal PSO solutions in providing actionable insights for microgrid developers and operators.

2. Background and Related Work

2.1. Microgrid Optimization Approaches

Microgrid optimization has been tackled through various methodologies, each with distinct strengths and computational trade-offs. Mixed-Integer Linear Programming (MILP) guarantees global optimality for convex problems but suffers from computational complexity in large-scale systems with nonlinear constraints. Moreover, some non-linear or variable constraints are not easy to set, potentially leading to loss of model realism. Meta-heuristic approaches such as Genetic Algorithms (GAs) and Particle Swarm Optimization (PSO) [7–10] handle non-convexity effectively and are widely adopted for their flexibility, though they provide no optimality guarantees and require careful parameter tuning. Commercial tools like HOMER have gained popularity for their user-friendly interface and rapid techno-economic assessment, yet remain limited to pre-defined component libraries and simulation-based optimization. A critical limitation across these methods is the prevalent reliance on single-objective formulations—typically minimizing Net Present Cost (NPC) or Levelized Cost of Energy (LCOE)—which fail to capture the multi-dimensional nature of rural electrification challenges. Such approaches often overlook crucial trade-offs between cost, reliability, environmental impact, and social acceptance, potentially leading to solutions that are economically optimal but practically unsuitable for off-grid contexts where resilience and community needs are paramount.

2.2. The PSO-MDO Methodology

Ref. [3] introduced a novel approach to microgrid sizing that allows PSO to identify several design options of the microgrid components by using an iterative approach that stores simulation data for each iteration. The key innovation lies in having all intermediate particle configurations evaluated during the PSO iterative process, not just the final optimal solution, in order to trace back other solutions in the "near-optimal" area, enhancing real application choice possibilities. The overall optimization workflow, including the PSO iteration loop and the yearly degradation tracking, is illustrated in Figure 2.

PSO for Microgrid Sizing: The PSO algorithm minimizes the system NPC, defined as:

$$\mathrm{NPC} = \mathrm{CAPEX} + \sum_{t=1}^{N_T} \frac{\mathrm{OPEX}_t}{(1+d)^t} \tag{1}$$

where N_T represents the project lifetime, d is the nominal discount rate, CAPEX includes investment costs, and OPEX encompasses operational expenses and fuel costs.

The optimization is therefore strictly single-objective:

$$x^* = argmin_x \; NPC(x)$$

with x = [PV_kW, BESS_kWh, Inv_kW, Gen_kW] bounded by the feasible ranges. No resilience, headroom or battery-health terms enter the objective, and consequently no interobjective weights, normalizations or penalty terms are defined. These criteria are evaluated in post-processing (Section 3.2) over the near-optimal set, not during the PSO search.

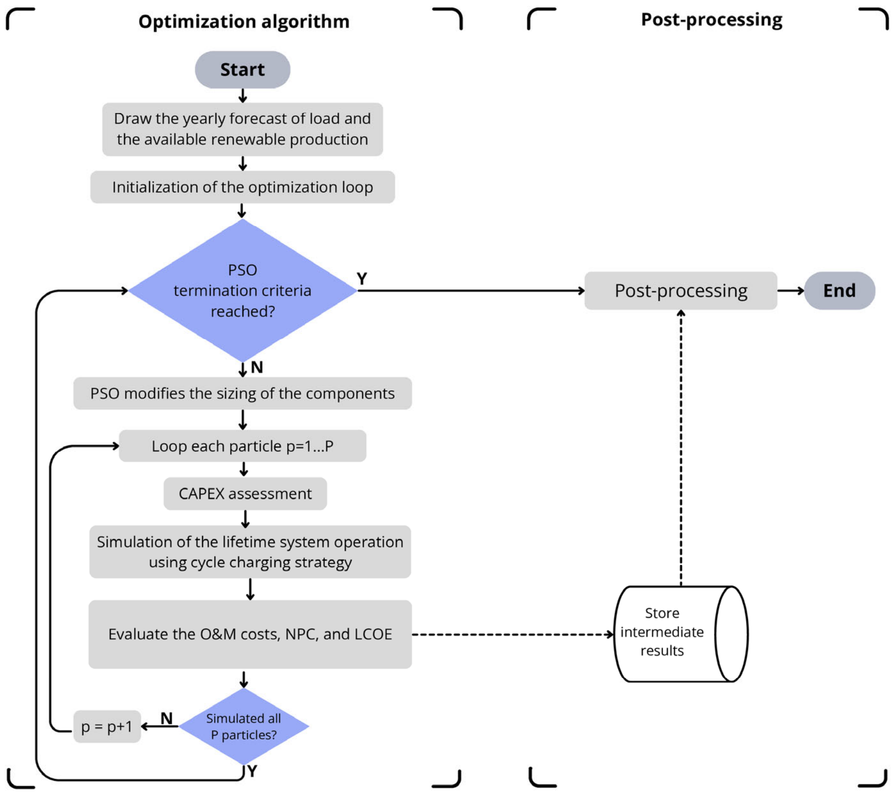

Figure 2. Optimization workflow showing PSO iteration loop with yearly degradation tracking and post-processing to extract representative designs. Each particle evaluation simulates 20 years of system operation at 15 min resolution.

Post-Processing for Multiple Designs: After PSO convergence, all evaluated particles within a preset NPC tolerance (5% for this study) from the optimal solution are retained. These near-optimal configurations are then visualized through color maps that reveal relationships between component sizes, fuel consumption, Energy Not Served (ENS), and initial investment, diesel generator share, average annual OPEX, average annual curtailment, battery cycling stress, delta fuel cost under demand growth and LCOE.

Limitation of Standard PSO-MDO: While the post-processing phase examines multiple metrics, the PSO search itself remains guided solely by NPC minimization. Consequently, the algorithm has no explicit mechanism to favor solutions with better resilience, lower battery stress, or greater capacity headroom during the optimization process.

2.3. Battery Health and Degradation Factors

Lithium-ion battery lifetime in stationary energy storage systems is governed by complex degradation mechanisms influenced by cell chemistry (the simulation uses LFP—Lithium Iron Phosphate cell chemistry parameters), as well as operational and environmental factors. Depth of Discharge (DoD) exhibits a non-linear relationship with cycle life: while shallow cycling (20–30% DoD) can extend battery life to several thousand cycles, deep discharges (80–100% DoD) accelerate capacity fade through increased mechanical stress on electrode materials and electrolyte decomposition. C-rate—the charge/discharge current relative to battery capacity—directly impacts both calendar and cycle aging, with high C-rates (higher than 1C) generating excessive heat and promoting lithium plating, which is particularly detrimental during charging phases. Temperature effects are perhaps the most critical yet often underestimated factor: elevated temperatures (higher than 35 °C) exponentially accelerate chemical degradation through Solid Electrolyte Interphase (SEI)-layer growth and active material dissolution, while low temperatures (lower than 10 °C) increase internal resistance and can cause irreversible lithium plating [1,3]. These factors interact synergistically, making lifetime prediction highly context-dependent. For off-grid microgrids in tropical or desert climates, thermal management becomes paramount, as the combination of high ambient temperatures and irregular charge/discharge patterns can reduce battery life by 40–60% compared to controlled laboratory conditions.

The mechanisms reviewed above (SEI growth, lithium plating, temperature-driven acceleration) motivate the design priorities of this study but are not all explicitly simulated. In this work, battery health is represented through two elements: (i) a phenomenological three-phase capacity-fade model applied year by year, and (ii) operational constraints and stress indicators on state of charge, depth of discharge and C-rate. Temperature effects and detailed electrochemical aging (SEI, lithium plating, loss of active material) are not modeled dynamically; they are used qualitatively to justify the conservative operating limits adopted. A remote, off-grid, replacement-constrained context calls for robust, conservative operating conditions. A detailed electrochemical aging model has limited direct use within the scope of this paper; moreover, it would require cell-level test data, which are not available for this installation.

3. Methodology: NPC-Based PSO-MDO with Use-Case Post-Processing

3.1. Optimization Workflow

The PSO workflow uses NPC as the single objective function; the use-case criteria are applied afterwards, in post-processing:

- Initialization: Generate P particles with random component sizes within feasible bounds.
- Simulation: For each particle, simulate annual system operation using cycling charging strategy.
- Evaluation: Calculate the objective f(x) = NPC(x) for each particle, where NPC is the 20-year lifecycle cost defined in Equation (1). Update: Adjust particle velocities and positions based on personal and global best values.
- Convergence: Terminate when f(x) improvement <0.1% for 15 consecutive iterations.
- Storage: Unlike standard PSO, retain all evaluated particles and their metrics.

The PSO was run with 100 particles and cognitive/social/inertia coefficients $c_1 = 2$, $c_2 = 1$, $w = 0.8$, for a maximum limit of 40 iterations. The search was terminated early when the best objective value improved by less than 0.1% over 15 consecutive iterations. Under these settings, the algorithm converged after 28 iterations, corresponding to 2800 evaluated particle configurations (100 particles × 28 iterations).

3.2. Post-Processing and Multi-Design Selection

Following PSO convergence, the post-processing phase identifies multiple near-optimal designs:

- Filter particles within tolerance band: $f(x) < (1 + \epsilon)\cdot f(x^*)$ where ϵ = 1–5%.
- Generate color maps showing relationships between:
    - Component sizes (PV vs. BESS);
    - Performance metrics (CF, DoD, C-rate);
    - Economic indicators (NPC, CAPEX).
- Identify Pareto-optimal solutions balancing multiple criteria.
- Present trade-off curves to decision-makers.

The post-processing procedure used to identify the near-optimal designs is summarized in Figure 3.

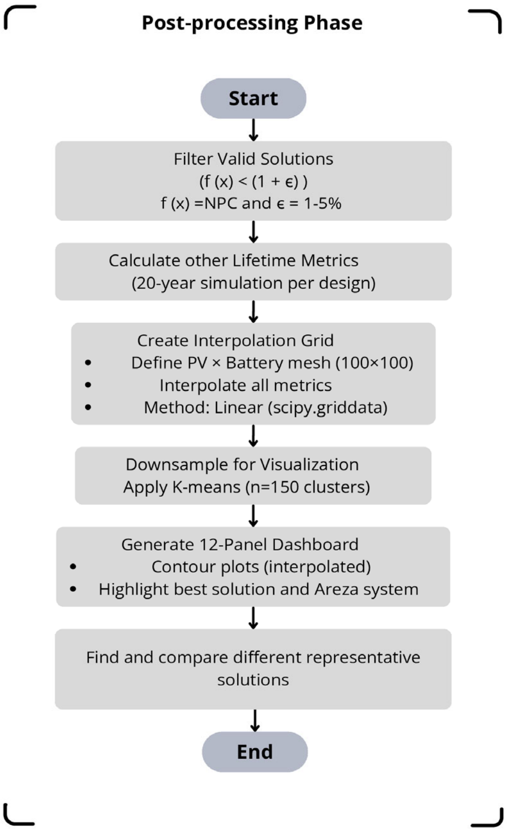

Figure 3. Post-processing phase flowchart.

4. Case Study Setup and Data

4.1. As-Built System Description

The technical specifications of the Areza system include the following:

- PV plant: 1.25 MWp;
- Battery Energy Storage System (BESS): Tesla Powerpack, 2310 kWh/460 kW;
- Four diesel backup generators of 400 kVA each;
- Diesel storage tank of 20,000 L;
- 415 V/15 kV transformer with a capacity of 1.25 MVA.

The system is part of a program supplying around 8900 households (≈41,000 residents) across the two towns of Areza and Maidma and 28 surrounding villages; this study focuses on the Areza site, which serves a share of that demand plus local commercial loads. A simplified single-line diagram of the Areza microgrid is shown in Figure 4.

4.2. Solar Resource

Solar PV is particularly suitable given the high solar insolation in Eritrea. A 2022 GIS-based estimation of solar energy potential in Eritrea resulted in an annual average maximum and minimum GHI of 2238 kWh/m^2 and 830 kWh/m^2 in the three regions in the lowlands (Ghash Barka, Northern Red Sea, and Southern Red Sea) [10], and an annual average maximum and minimum GHI of 2775 kWh/m^2 and 870 kWh/m^2 in the three regions in the highlands (Maekel, Anseba, and Debub, where Areza is located).

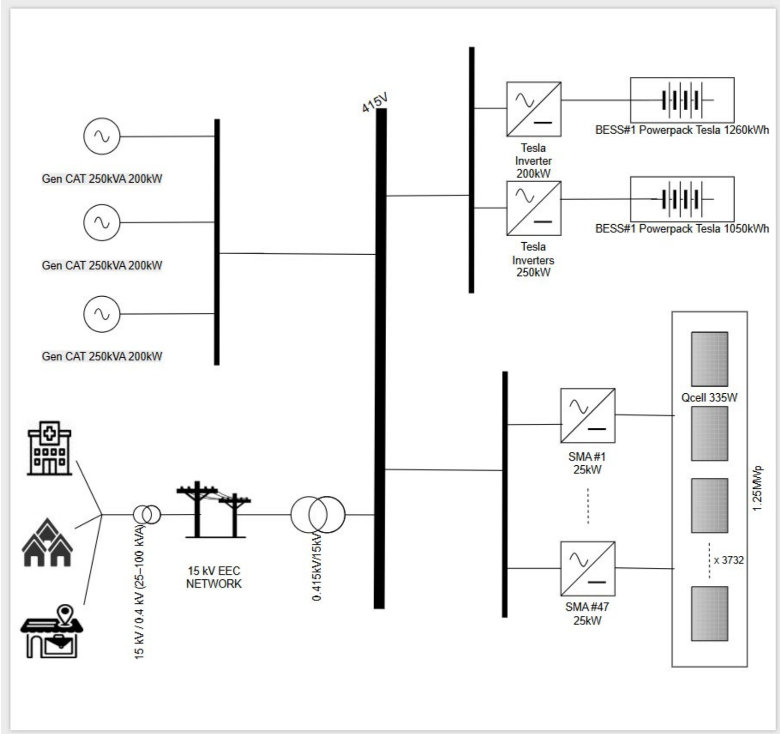

Figure 4. Areza simplified single-line diagram.

For the Areza case study, Table 1 summarizes long-term monthly and daily irradiation indicators (from SolarGIS [11]—used for monthly/daily irradiation indicators). NASA POWER [12] was used as the source of the hourly dataset applied to the analysis. See Section 4.6 together with the average diurnal air temperature.

Table 1. Areza data summary. G_{h_m} is monthly sum of global irradiation [kWh/m^2], G_{h_d} is daily sum of global irradiation [kWh/m^2], D_{h_d} is daily sum of diffuse irradiation [kWh/m^2], and T_{24} is daily (diurnal) air temperature [°C].

Month	G_{h_m}	G_{h_d}	D_{h_d}	T_{24}
January	188	6.07	1.39	19
February	190	6.77	1.63	20.6
March	224	7.22	1.97	22.4
April	211	7.02	2.31	24
May	208	6.71	2.6	24.9
June	184	6.14	3.02	22.7
July	153	4.92	3	19.1
August	142	4.58	2.87	18.7
September	176	5.86	2.73	21.4
October	191	6.17	2.08	21.7
November	179	5.98	1.54	20.3
December	179	5.78	1.36	19.2
Year	2225	6.09	2.21	21.2

4.3. Operational Data Collection

SCADA data were collected from the Areza microgrid over a 14-month period (October 2023 until November 2024), with 5 min sampling resolution. Key parameters monitored include:

- Load demand (kW, kWh);
- PV generation (kW);

- BESS state of charge (%);
- BESS power flow (kW, positive = charge, negative = discharge).

Gap-Filling Methodology

The raw 5 min demand time series contained missing samples and occasional zero values. These artifacts were treated as a data-quality issue (rather than physical demand curtailment), since the optimization framework aims to size a system that delivers continuous service. We adopted a pattern-based reconstruction method based on recurrent weekly consumption rhythms.

First, we identified a subset of "clean" months (defined as months with more than 90% valid non-zero measurements) and used them to build a reference database. In the Areza dataset, seven months met this threshold (October 2023, December 2023, and February–June 2024), providing 90,987 valid measurements. For each combination of day of week $d \in \{1, \ldots, 7\}$ and hour of day $h \in \{0, \ldots, 23\}$ (168 bins), we computed the mean load $\mu_{d,h}$ from the reference data:

$$\mu_{d,h} = \mathbb{E}[P(t) \mid \mathrm{dow}(t) = d,\ \mathrm{hod}(t) = h,\ t \in \mathcal{R}],$$

where $\mathcal{R}$ is the set of timestamps belonging to clean months and with non-zero measurements.

Then, for each missing or suspicious record (NaN or zero), the load value was replaced by the corresponding $\mu_{d,h}$ of its time slot (same day of week and hour of day).

Table 2 presents key statistics before and after gap filling.

Table 2. Load data statistics before and after gap filling.

Metric	Before	After	Change
Valid records	90,987	114,625	+23,638
Mean load (kW)	155.7	146.1	−9.6 (−6.1%)
Std. deviation (kW)	89.1	88.8	−0.3
Median (kW)	149.5	142.0	−7.5
Maximum (kW)	589.4	589.4	0.0
Total energy (GWh)	1.180	1.396	+0.215 (+18.3%)

The "before" and "after" columns are computed on different sample sets: "before" uses only the valid, non-zero measurements (90,987 records), whereas "after" uses the complete reconstructed timeline (114,625 records). This explains the apparently counter-intuitive combination of a lower mean and a higher total energy. Per-sample statistics (mean, median, standard deviation) are intensive quantities, while record count and total energy are extensive (aggregate) quantities, so the two need not move in the same direction. By construction, the 23,638 reconstructed samples carry an average load of ≈109 kW—below the 155.7 kW mean of the valid samples—which lowers the overall per-sample mean; at the same time, these intervals, previously recorded as missing or zero and therefore contributing no energy, are now assigned their expected demand, which raises the aggregate total energy by 18.3%. The maximum (589.4 kW) is unchanged, since reconstruction never exceeds observed peaks.

The gap-filling procedure reconstructs missing intervals using conditional mean profiles (binned by day type and hour) estimated from the valid measurement period. By construction, this preserves the diurnal and seasonal shape of the load, which is the property most relevant to relative component sizing. The 18.3% increase in total energy reflects the recovery of intervals missing from the raw record due to metering downtime, with no significant plant outages in the gaps; it is therefore not an inflation of per-interval demand but a more complete estimate of annual served energy, and using the raw record would bias the sizing downward.

4.4. Load Characterization

The aggregated daily profile in Figure 5 shows a progressively rising demand from the early morning, until the first local maximum between 10 and 11 AM, and a definite evening shoulder around 19:00–20:00. The blue shaded band representing the standard deviation clearly shows high dispersion at midday, probably indicating intermittent commercial activity; in contrast, the evening shoulder is more stable, plausibly driven by residential lighting and appliance use. While the maximum load power measured is 600 kW, the average midday peak is 250 kW and 200 kW in the evening shoulder.

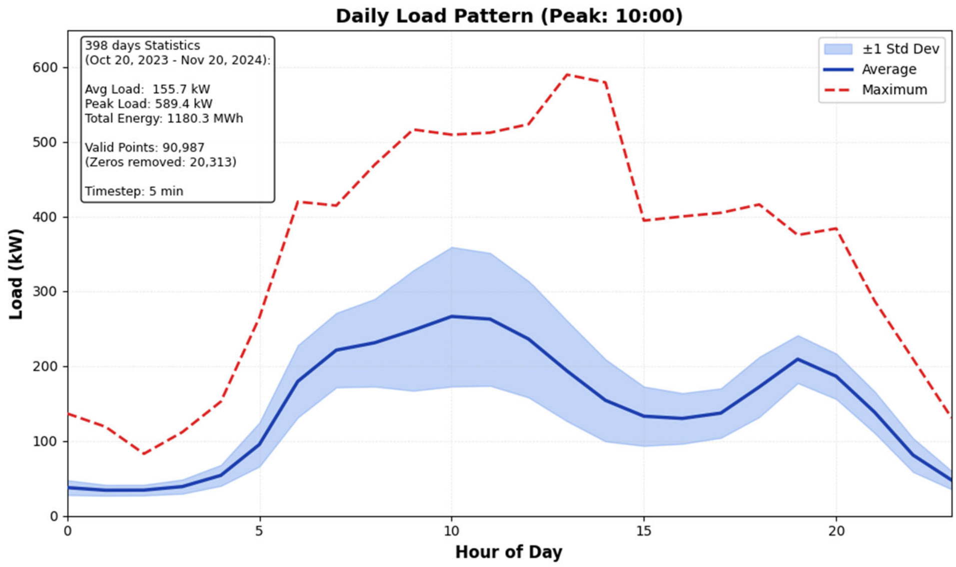

Figure 5. Daily load profile of the Areza microgrid (before filling data).

The seasonal variation in the hourly load demand across months is illustrated by the heatmap in Figure 6, whereas Figure 7 compares, on a monthly basis, the original measured data with the reconstructed (gap-filled) series.

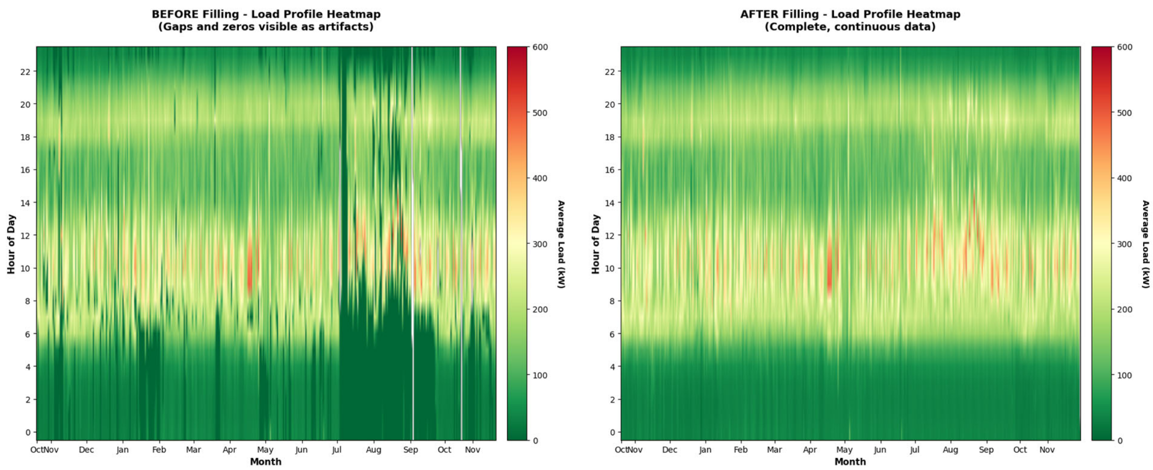

Figure 6. Heatmap comparison of hourly load demand patterns across months, showing seasonal and diurnal variations in the Areza microgrid.

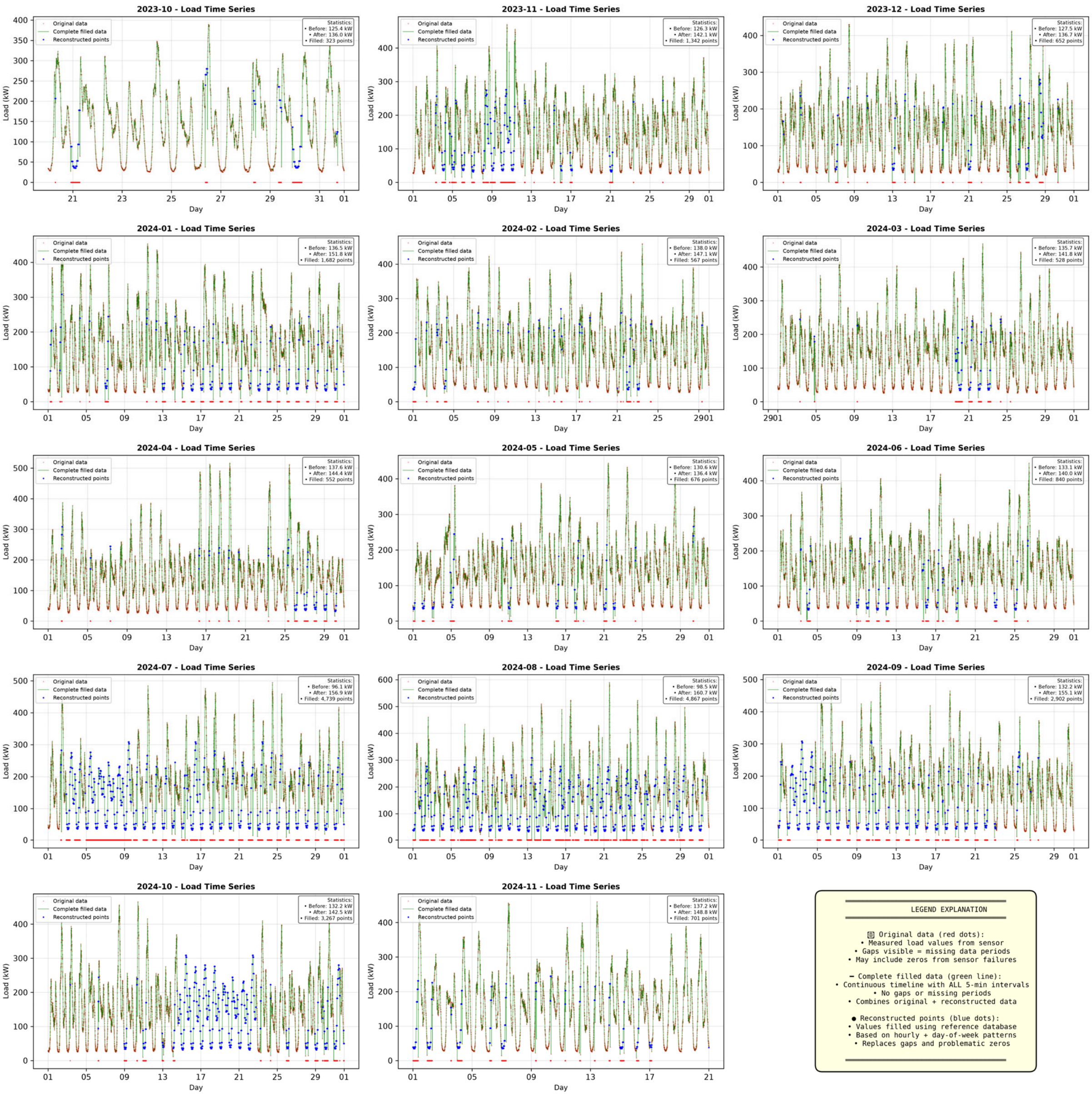

Figure 7. Monthly time-series comparison showing original measured data (red dots, with visible gaps), complete filled timeline (green line), and reconstructed points (blue dots) for all 14 months of the study period.

4.5. Cost Parameters and Assumptions

A summary of all the technical and economic assumptions is shown in Table 3.

LCOE Calculation

The Levelized Cost of Energy (LCOE) was calculated following the HOMER approach, which converts the total Net Present Cost (NPC) into an equivalent annual cost using the Capital Recovery Factor (CRF) and dividing by the annual energy served (HOMER Energy, n.d.) [13].

$$\mathrm{CRF}(i,N) = \frac{i(1+i)^N}{(1+i)^N - 1}$$

where i is the annual nominal discount rate and N is the project lifetime in years. For $i = 8\%$ and $N = 20$, $\mathrm{CRF}(0.08, 20) = 0.1019$.

$$\mathrm{LCOE} = \frac{\mathrm{CRF}(i, N)\, C_{\mathrm{NPC}}}{E_{\mathrm{annual}}}$$

where C_{NPC} is the total net present cost [EUR] and E_{annual} is the annual energy served [kWh/year].

Table 3. Economic and technical assumptions used in simulation.

Item	Value
Nominal discount rate	8%
Project lifetime	20
Diesel price (year 1)	EUR 1.00/L; escalation 3%/y
ENS penalty	EUR 100/kWh
O&M escalation	2%/y
PV performance ratio	0.85
PV degradation	0.6%/y
BESS degradation	Years 1–10: 0.8%/y; years 11–15: 1.2%/y; years 16–20: 2.0%/y
BESS SoC limits	10–90% (init. 50%)
Charge/discharge efficiency	95%/95% (AC basis)
Generator loading window	30–70% (cycle charging)
Gen start/stop SoC	10%/20%
O&M (PV, BESS, inverter, genset)	1.5%, 2.0%, 2.5%, 2.0% of CAPEX/yr
CAPEX (PV, BESS, inverter, genset)	EUR 600/kW, EUR 230/kWh, EUR 160/kW, EUR 500/kW
Timestep	15 min

In the case of Areza, the minigrid program was co-funded by the European Union and the Government of Eritrea, with additional financing from the United Nations Development Programme (UNDP) (European External Action Service (EEAS) n.d.). Therefore, in this study, the NPC is computed using nominal cash flows (diesel escalation 3%/y and O&M escalation 2%/y) discounted with a nominal discount rate of $i = 8\%$ (Table 3). That would result in a real discount rate of $\pm 6\%$, which supports interpreting the economic assumption with relatively favorable financial conditions.

4.6. Simulation Tool and Implementation

The optimization framework was implemented in Python 3.11, using open-source scientific computing libraries. Core simulation and optimization routines employed NumPy (v1.24+) for numerical operations and Pandas (v2.0+) for time-series data handling and resampling. The particle swarm optimization (PSO) algorithm was implemented with PySwarms (v1.3.0) [14], which allows for flexible customization of swarm parameters and constraint handling.

Visualization and analysis were performed using Matplotlib (v3.7+) to generate high-quality figures and plots. Configuration management was achieved using YAML files parsed by PyYAML (v.6.0+), enabling reproducible scenario definitions and parameter sweeps without hard-coding values in the source code. Energy system modeling and economic calculations were developed using custom functions built on these frameworks.

Post-processing of MDO results used scikit-learn (v1.3+) for k-means clustering of representative designs and SciPy (v1.11+) for Delaunay-based linear interpolation of performance metrics across the design space. The unified 12-plot dashboard displays interpolated contours of net present cost (NPC), levelized cost of energy (LCOE), curtailment, and battery cycling on a 100×100 grid in the PV–battery plane.

Weather data preprocessing uses pvlib-python (v0.10+), which relies on established models for calculating solar position, irradiance transposition, and plane-of-array (POA) geometry. The library handles the conversion from horizontal irradiance components to tilted-plane irradiance using the Perez transposition model (Perez et al. 1990) [15]. Since the NASA POWER (see Section 4.2) dataset provides only global horizontal irradiance (GHI) at hourly resolution, we used pvlib's DISC model (Maxwell 1987) [16] to decompose GHI into direct normal irradiance (DNI) and diffuse horizontal irradiance (DHI) components before applying the transposition.

Temporal interpolation to convert hourly irradiance data to 15 min resolution was performed using Pandas' native *.resample()* and *.interpolate(method='linear')* functions. In the same way, electrical load data aggregation from 5 min to 15 min resolution was carried out with Pandas' *.resample('15T').mean()* method to compute arithmetic averages.

4.7. Multi-Year Dispatch Simulation

Rather than simulating a single representative year and multiplying costs by 20, we explicitly model each year from 2024 through 2043. This captures the gradual decline in system performance as components age.

Solar panels lose approximately 0.6% of their output capacity per year due to cell degradation and soiling accumulation. By year 20, the PV array delivers 84% of its nameplate rating.

Battery degradation follows a three-phase model, with annual capacity-loss rates of 0.8% (years 1–10), 1.2% (years 11–15) and 2.0% (years 16–20), reflecting the accelerating, non-linear nature of lithium–iron–phosphate aging reported in the literature (Severson et al. 2019 [17]). We note that empirical LFP studies typically place the onset of accelerated fade at lower states of health; the rates adopted here are therefore a deliberately conservative parametrization rather than a calibration to a specific dataset, appropriate for a deployment context (remote, off-grid, replacement-constrained) where overestimating degradation is preferable to underestimating it.

We cap the minimum usable capacity at 50% to prevent the optimizer from exploiting unrealistic degradation paths.

This 50% value is a numerical floor on the simulated degraded capacity, not an operational limit on usable energy or an end-of-life threshold. Under the three-phase degradation model adopted here, the retained capacity at year 20 remains well above this level, so the floor is never binding for realistic designs; it acts only as a safeguard preventing the optimizer from exploiting non-physical degradation trajectories in the search space.

Each year's simulation runs at 15 min resolution using actual 2023–2024 load and solar data. The dispatch logic implements a cycle-charging strategy where the battery serves as the primary buffer between solar generation and demand. When solar exceeds load, excess energy charges the battery up to 90% state of charge. When load exceeds solar, the battery discharges down to 10% SOC. The diesel generator activates only when both solar and battery cannot meet demand, or when the battery requires recharging during extended cloudy periods.

Generator dispatch includes minimum and maximum loading constraints (30–70% of rated capacity) to reflect realistic operational limits. Operating a diesel engine below 30% load results in incomplete combustion and accelerated wear, while operating above 70% load risks overheating and reduces fuel efficiency. Fuel consumption uses a model where efficiency degrades sharply below 45% loading (0.30 L/kWh at 30–45% loading versus 0.25 L/kWh at 60–70% loading). Because the load is relatively small during the night, the generator starts when the battery reaches 10% state of charge, supplies the load operating at the highest efficiency point, and charges the battery with the excess until

20% state of charge. Then the battery takes over, and the cycle is repeated. This is necessary to maximize generator efficiency. An example of the dispatch strategy is shown in Figure 8.

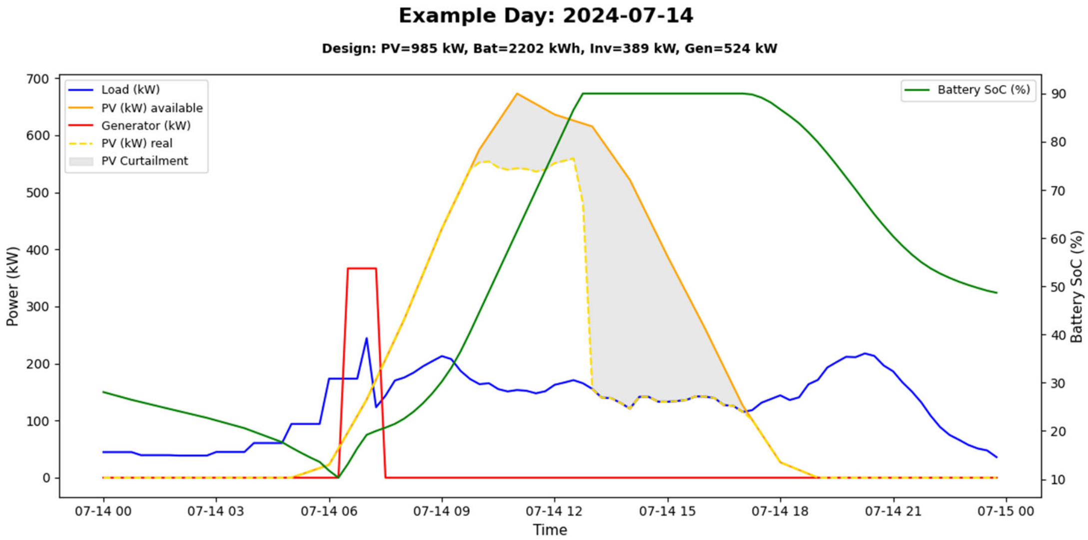

Figure 8. Example day dispatch results (15 min resolution) for the selected microgrid design. The left axis shows power flows: the electrical load (blue), available PV power (orange), PV power used after curtailment (yellow dashed), and diesel generator output power (red). The grey shaded area indicates PV curtailment, i.e., the portion of available PV that is not injected because demand is already met and the battery is constrained by its power/energy limits. The battery state of charge (green) is shown on the right axis, highlighting daytime charging from PV surplus and evening/night discharge to support the load and reduce generator runtime.

Strategy Equations

At each timestep t, the system balances power flows according to the following priority hierarchy:

1. Net load calculation

$$P_{\text{net}}(t) = P_{\text{load}}(t) - P_{\text{pv}}(t).$$

2. Battery dispatch

$$\begin{aligned} \text{If } P_{\text{net}}(t) > 0(\text{deficit}): \quad & P_{\text{bat}}^{\text{dis}}(t) = \min\left\{P_{\text{net}}(t),\ P_{\text{inv}},\ C_{\text{rate}}\,E_{\text{bat}},\ \frac{\text{SoC}(t)-\text{SoC}_{\text{min}}}{\eta_{\text{dis}}\,\Delta t}\right\} \\ \text{If } P_{\text{net}}(t) \le 0(\text{surplus}): \quad & P_{\text{bat}}^{\text{ch}}(t) = \min\left\{|P_{\text{net}}(t)|,\ P_{\text{inv}},\ C_{\text{rate}}\,E_{\text{bat}},\ \frac{\text{SoC}_{\text{max}}-\text{SoC}(t)}{\eta_{\text{ch}}\,\Delta t}\right\} \end{aligned}$$

3. State-of-charge update

$$\text{SoC}(t+1) = \text{SoC}(t) + P_{\text{bat}}^{\text{ch}}(t)\,\eta_{\text{ch}}\,\Delta t - \frac{P_{\text{bat}}^{\text{dis}}(t)}{\eta_{\text{dis}}}\,\Delta t.$$

4. PV curtailment
If $\text{SoC}(t) \ge 90\%$ *and* $P_{\text{pv}}(t) > P_{\text{load}}(t)$, then:

$$P_{\text{curtail}}(t) = \max\left\{0,\ P_{\text{pv}}(t) - P_{\text{load}}(t) - P_{\text{inv}}\right\}.$$

5. Generator dispatch

$$\text{DGonif SoC}(t) \le 10\% \text{ or } P_{\text{net}}(t) - P_{\text{bat}}^{\text{dis}}(t) \ge 0.30\,P_{\text{gen}}^{\text{rated}}.$$

When on, enforce the optimal loading window:

$$P_{\text{gen}}(t) \in \left[0.30\, P_{\text{gen}}^{\text{rated}},\ 0.70\, P_{\text{gen}}^{\text{rated}}\right].$$

6. Fuel consumption

$$\lambda(t) = \frac{P_{\text{gen}}(t)}{P_{\text{gen}}^{\text{rated}}}, \qquad \text{Fuel}(t) = P_{\text{gen}}(t)\, \alpha(\lambda)\, \Delta t,$$

with specific fuel consumption (L/kWh):

$$\alpha(\lambda) = \begin{cases} 0.25, & \lambda \geq 0.60 \text{ (optimal)}, \\ 0.27, & 0.45 \leq \lambda < 0.60, \\ 0.30, & 0.30 \leq \lambda < 0.45, \\ 0.40, & \lambda < 0.30 \text{ (inefficient)}. \end{cases}$$

7. Energy Not Served (ENS). If unmet demand persists after battery and generator dispatch, define:

$$\text{ENS}(t) = \max\left\{0,\ P_{\text{net}}(t) - P_{\text{bat}}^{\text{dis}}(t) - P_{\text{gen}}(t)\right\}.$$

The notation used throughout this section is summarized in Table 4.

Table 4. Notation summary.

Symbol	Description	Units
$P_{\text{load}}(t)$	Electrical load demand	kW
$P_{\text{pv}}(t)$	PV power available	kW
$P_{\text{net}}(t)$	Net load (deficit/surplus)	kW
$P_{\text{bat}}^{\text{dis/ch}}(t)$	Battery discharge/charge power	kW
P_{inv}	Inverter power rating	kW
$P_{\text{gen}}(t)$	Generator output power	kW
$\text{SoC}(t)$	State of charge	%
E_{bat}	Battery capacity	kWh
C_{rate}	Battery C-rate (e.g., $0.5\,\text{h}^{-1}$)	
$\eta_{\text{ch}}, \eta_{\text{dis}}$	Charge/discharge efficiency	
Δt	Timestep (e.g., 0.25 h)	h
$\alpha(\lambda)$	Specific fuel consumption	L/kWh

The simulation tracks several key metrics for each year:

- Annual fuel consumption (liters);
- Total Energy Not Served (kWh);
- Component degradation states (percentage of original capacity);
- Diesel generation share (percentage of total annual demand);
- Total PV energy curtailed;
- Average DoD.

The dispatch model described above is rule-based: it assumes a cycle-charging strategy with fixed state-of-charge thresholds (charging to 90%, discharging to 10% SoC) and generator loading limits (30–70% of rated power). These rules approximate the control policy of the Areza installation, but they cannot be directly verified: the actual dispatch logic resides in the inverter firmware and the control actions are not logged in the available SCADA records, which capture observable states (PV output, load, battery state of charge, power flows) rather than control decisions. The assumed strategy can therefore be inferred from, but not confirmed against, the measured data. Because dispatch assumptions directly affect diesel use, curtailment, battery cycling and unmet energy, the present results should be read as the outcome of an assumed, transparent operating strategy—a standard choice in sizing studies—rather than of a validated digital twin of Areza. A behavioral comparison of simulated and recorded observable quantities (PV output, load, battery state of charge, generator usage), and the reconstruction of the underlying control policy where additional instrumentation becomes available, are identified as priorities for future work.

5. Results and Analysis

5.1. NPC-Optimal Baseline Design

The PSO was run with 100 particles and cognitive/social/inertia coefficients $c_1 = 2$, $c_2 = 1$, $w = 0.8$ for a maximum of 40 iterations. The search was terminated early when the best objective value improved by less than 0.1% over 15 consecutive iterations. Under these settings, the algorithm converged after 28 iterations, corresponding to 2800 evaluated particle configurations (28 iter $\times$ 100 particles each). The key performance indicators of the optimization are summarized in the MDO–PSO dashboard shown in Figure 9.

The optimal configuration, with NPC-only optimization, is:

- PV: 973 kW;
- BESS: 2236 kWh/392 kW;
- Generator: 522 kW;
- NPC: EUR 2.02 M;
- LCOE: EUR 0.161/kWh.

Having established the least-cost configuration, we now examine the near-optimal region surrounding it, where the use-case post-processing is applied.

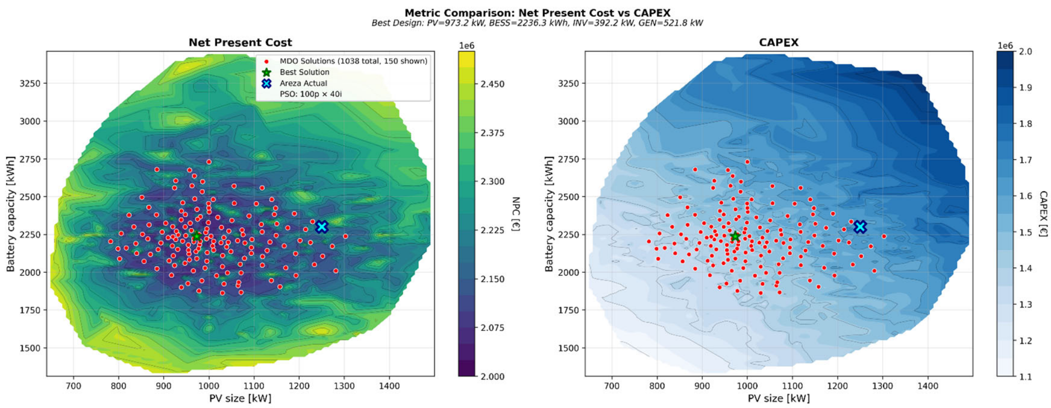

Figure 9. *Cont.*

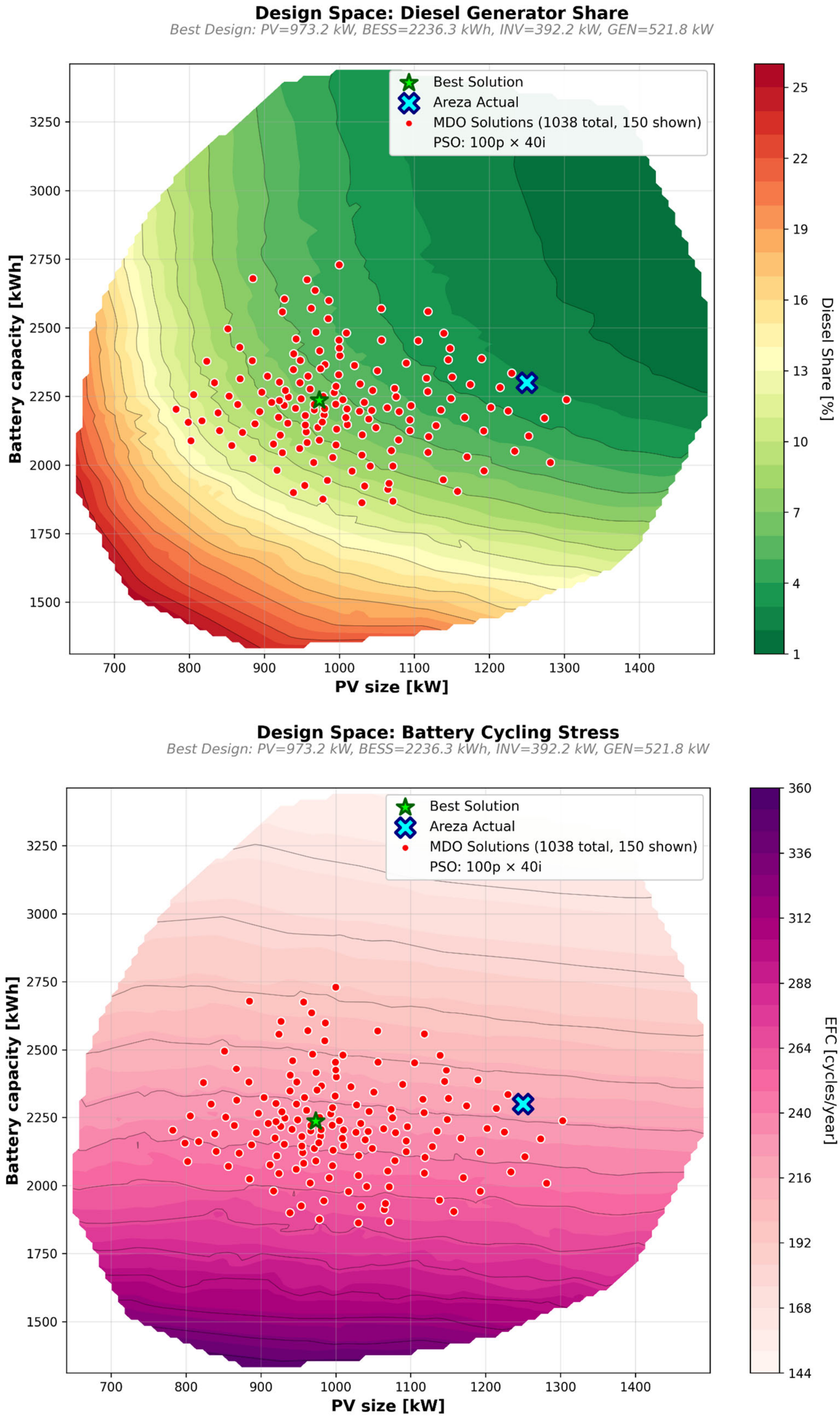

Figure 9. MDO–PSO dashboard for the Areza sizing study. Key performance indicators across the explored design space; the best solution and current Areza system are marked with a star and a cross, respectively. PSO settings: $c_1 = 2$, $c_2 = 1$, $w = 0.8$ (100 particles, 40 iterations).

5.2. The Near-Optimal Region: Use-Case Post-Processing

The post-processing phase identified six design configurations within 5% tolerance of the optimum.

This portfolio reveals:

- PV capacity ranges from 780 to 1320 kWp;
- BESS capacity ranges from 1760 to 2750 kWh;
- BESS inverter ranges from 328 to 793 kW;
- Diesel generator size relatively constrained to 467–679 kW;
- Strong trade-off visible between PV size and battery stress, as summarized by Table 5.

Table 5. Sizing flexibility within the 5% NPC band (MDO set), expressed as deviation from the best design. The downward deviation is $\Delta^- = (x_{best} - x_{min})/x_{best}$, and the upward deviation is $\Delta^+ = (x_{max} - x_{best})/x_{best}$.

Parameter	Range	Best Design	Δ^-	Δ^+
PV capacity [10 kW]	780–1320	973	19.8%	35.7%
Battery capacity [kWh]	1760–2750	2236	21.3%	23.0%
Battery inverter [kW]	328–793	392	16.3%	102.3%
Generator sizing [kW]	467–679	522	10.5%	30.1%

The scatterplot in Figure 10 places all 150 K-means solutions (gray dots) alongside the seven selected representatives (colored markers). The representatives generally span the design space rather than clustering in one region. The NPC Optimal design sits near the center-left, while Fuel Risk Hedge/Productive Use occupies the right side and Battery Life and Demand Robust the center-top area. Low-CAPEX predictably lands in the lower left.

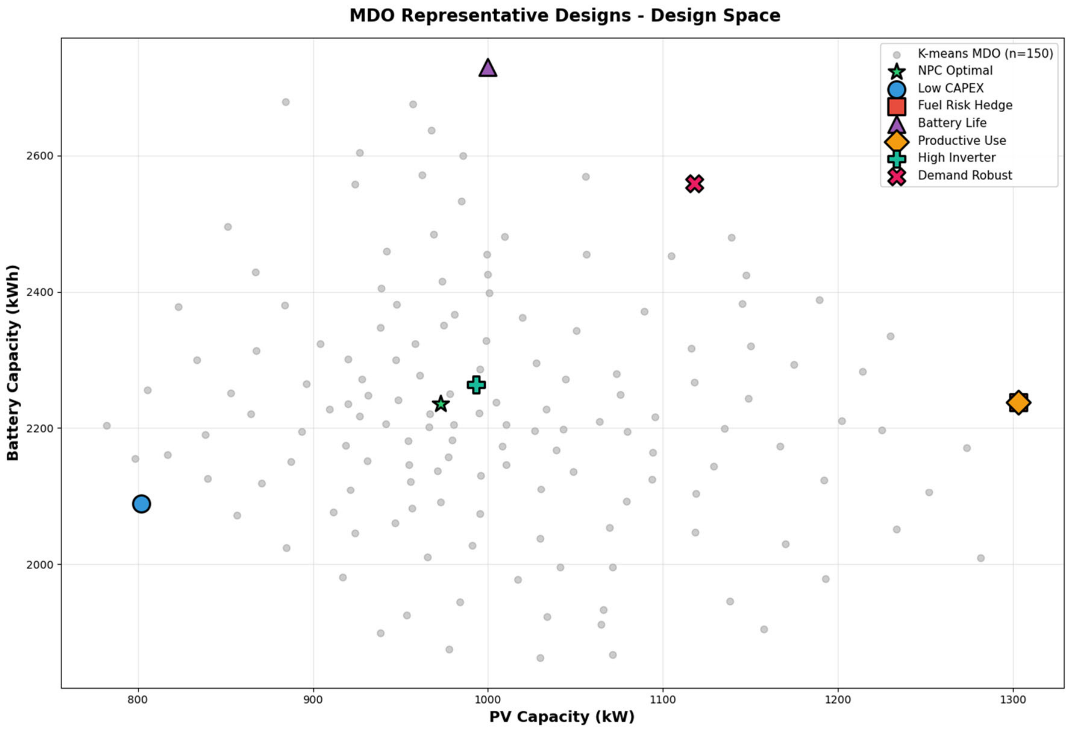

Figure 10. Strategic comparison of representative designs selected from the MDO set (K-means downsampled set, $n = 150$) in the PV–battery design space relative to the downsampled MDO cloud.

This spatial diversity validates the selection methodology. A simplistic approach might cluster representatives near the NPC minimum; the strategic selection instead ensures that decision-makers see the full range of viable options and can match them with their current project needs.

The following table synthesizes the key trade-offs across the seven representative designs.

Each representative design is selected from the near-optimal set as the configuration that best satisfies a specific use-case priority while remaining within the 5% NPC tolerance band: NPC_Optimal is the cost minimum, Low_CAPEX minimizes upfront investment, Fuel_Risk_Hedge/Productive_Use maximizes PV headroom to reduce diesel reliance, Battery_Life minimizes battery cycling stress, High_Inverter maximizes instantaneous power capability, and Demand_Robust maximizes tolerance to load growth. Where two priorities are best served by the same near-optimal configuration, that configuration is listed once under both labels.

Against this portfolio of optimized designs, we now position the system as actually built in Areza.

5.3. Comparison with the As-Built Areza System

The comparison with the Areza actual system (PV = 1250 kW, battery = 1900 kWh, inverter = 450 kW, generator = 600 kW) is instructive. The Areza configuration lies outside the optimal MDO region, particularly in its oversized PV and generator, yet remains within roughly 8–10% of optimal NPC. Most surprisingly, it lies between the Fuel Risk Hedge/Productive Use designs and Demand Robust in Figure 10. This suggests that the actual installation may have been sized with reliability margins, reduced diesel dependency, or demand growth anticipation that the pure cost optimization does not capture.

The nature of this oversizing can be characterized directly from the design vectors, without additional simulation. Relative to the NPC-optimal design, the as-built system carries roughly +28% PV capacity and +15% generator capacity, while using a 15% smaller battery; the additional capacity is therefore concentrated in generation and backup rather than in storage. This is consistent with a robustness-oriented rationale rather than a least-cost one: as shown by the NPC–CAPEX asymmetry (Section 6), oversizing PV and generation acts as low-cost insurance against fuel-price exposure and demand growth, whereas undersizing them raises NPC sharply through diesel reliance. Consistent with this, the as-built configuration tolerates approximately +16% load growth before reaching the energy-adequacy limit (Section 5.2), i.e., it embeds headroom that a strictly least-cost design does not. On the storage side, the as-built battery operates at structurally low current stress (C-rate $\leq$ 0.5C in all conditions) but at comparatively deep average depth of discharge (~57%); this combination is consistent with LFP chemistry, which tolerates deep discharge relatively well while being more sensitive to high current and thermal stress. A full, single-simulation comparison of both designs across all operational indicators (fuel use, curtailment, unmet energy, battery cycling, load-growth tolerance and battery stress) under identical assumptions is the natural next step and is left to future work. With the present evidence, the as-built system is best understood as robustness- and reliability-oriented rather than simply oversized.

Beyond this steady-state comparison, we next assess how the as-built system responds to progressive load growth.

5.4. Preliminary Breaking-Point Analysis

Progressive load growth scenarios reveal system capacity limits. Breaking points are defined, where:

- Energy unmet > 10% of total demand;
- Battery DoD > 85% for > 15% of time;
- C-rate > 1.0 for > 5% of time.

For the as-built Areza system:

Under progressive load growth, the as-built system (1.25 MWp PV, 1.9 MWh BESS) is characterized as follows. Energy adequacy is the first binding constraint: unmet energy rises from about 3.2% of annual demand at current load to the 10% adequacy threshold at approximately +16% load growth (no PV expansion). Battery current stress never becomes binding: the C-rate remains below 0.5C across all tested load-growth levels (up to +100%). Depth-of-discharge stress, by contrast, increases steadily—the share of time spent below 15% state of charge (DoD > 85%) rises from ~16% at current load to ~65% at +100% growth, and average per-cycle DoD increases from ~57% to ~80%. Notably, deep-discharge stress is already significant at present load, indicating that the as-built battery operates with a limited reserve margin even before any load growth. A full quantification of a depth-of-discharge breaking point, of the corresponding thresholds for every design in the near-optimal portfolio, and of the recovery capacity (PV, storage or generator addition) required to restore acceptable performance is the subject of ongoing work.

Taken together, these results translate into the practical sizing guidance summarized below.

5.5. Practical Design Recommendations

The combination of a wide near-optimal region and the use-case post-processing translates into concrete guidance for developers. Because NPC varies by only about 5% across the near-optimal set while CAPEX spans nearly 28%, the choice among the representative designs (Table 6) can be driven by project priorities rather than by cost alone, with little economic penalty. For capital-constrained projects, the Low_CAPEX design minimizes upfront investment, at the cost of a higher diesel share. Where fuel-price exposure or future productive loads are the main concern, the Fuel_Risk_Hedge/Productive_Use design adds PV headroom that lowers diesel reliance, accepting greater curtailment as a reserve for demand growth. Where battery longevity dominates—the typical situation in remote, maintenance-constrained sites such as Areza—the Battery_Life design reduces cycling stress through additional storage. The Demand_Robust design is preferable where significant load growth is anticipated, and the High_Inverter design where high instantaneous power demand is expected.

Table 6. Representative (most common criteria of plant design functional optimization, based on specific use case) MDO strategies: sizing, cost, and operational indicators (lifetime).

Strategy	PV	Bat	Inv	Gen	NPC	CAPEX	LCOE	Diesel	Curtail	EFC	ΔFuel
	kW	kWh	kW	kW	EUR M	EUR M	EUR c/kWh	%	MWh/y	cyc/y	EUR k/y
NPC_ Optimal	973	2236	392	522	2.02	1.43	16.1	6.7	424	231	26
Low_ CAPEX	802	2088	349	525	2.12	1.28	16.8	12.8	197	247	46
Fuel_Risk_Hedge/Productive Use	1303	2238	373	492	2.12	1.61	16.8	3.0	954	224	14
Battery_Life	1000	2730	399	537	2.12	1.58	16.8	4.4	444	192	15
High_Inverter	993	2264	755	528	2.11	1.51	16.7	6.2	452	228	24
Demand_Robust	1118	2559	488	533	2.12	1.62	16.9	3.3	637	201	12

ΔFuel (EUR k/y): additional annual fuel expenditure incurred by each design under a +20% demand-growth scenario, relative to its baseline-demand fuel cost. Lower values indicate greater robustness to load growth.

Two cross-cutting principles emerge. First, the CAPEX–fuel asymmetry favors erring toward oversizing PV and storage: undersizing is penalized sharply through lifetime fuel costs, whereas modest oversizing is comparatively inexpensive insurance against fuel-price risk and demand growth. Second, for LFP storage in hot, replacement-constrained contexts, keeping the C-rate low—as observed throughout this study—is an effective and low-cost lever for battery health, even when depth of discharge is relatively deep. These recommendations derive from a preliminary, single-site analysis and should be confirmed by the sensitivity and validation studies identified as future work.

6. Discussion

This work proposed and applied a multi-design optimization (MDO) framework, combined with particle swarm optimization (PSO), to explore the sizing trade-offs of an off-grid PV–battery–diesel microgrid for the Areza case study. Rather than producing a single "optimal" design, the results highlight a near-optimal region in which substantially different component combinations achieve similar lifecycle economic outcomes.

The main conclusions can be summarized as follows:

1. **Near-optimal designs form a wide decision space, not a single point.** Across the design set, the Net Present Cost (NPC) varies by only $\sim$ 5 %, while CAPEX spans nearly $\sim$ 28%. Practically, this means that developers can freely choose sizing strategies that align with financing constraints, risk tolerance, and expansion plans, without significantly increasing lifecycle costs.
2. **NPC is primarily shaped by the CAPEX–fuel trade-off, and the penalty is asymmetric.** Undersizing PV or storage pushes the system into high diesel reliance, and NPC rises quickly because fuel accumulates and increases over the project lifetime. After the analysis, this is even clearer in the MDO-Pareto front (Figure 11), where a reduction in CAPEX of $\sim$ 9 % from the optimal solution causes a maximum increase in lifetime cost, while for the same lifetime cost you can increase the CAPEX by $\sim$ 14%, with all the benefits of an oversized system. The economic results rest on a fixed set of assumptions (Table 3), and we did not perform a formal sensitivity analysis on them; this is a preliminary evaluation whose primary aim is to test a use-case customization of the PSO–MDO methodology rather than to deliver definitive sizing recommendations. We note, however, that the central qualitative finding—the existence of a flat near-optimal region in which NPC varies little while CAPEX varies substantially—follows from a structural mechanism: near the optimum, the higher investment of an oversized design is offset over the project lifetime by lower fuel and OPEX, so NPC stays nearly constant while CAPEX changes. This compensation is expected to hold across a broad range of parameter values; what economic assumptions mainly shift is the width and center of the near-optimal region, not its existence. A formal sensitivity analysis on diesel price, discount rate, PV and BESS CAPEX, and the ENS penalty—which would quantify these shifts and confirm the robustness of the recommendations—is left to future work.
3. **Low diesel share often comes with higher curtailment: fuel risk can be limited, but not for free and not entirely.** Designs that minimize diesel share typically carry more PV headroom than the fixed demand can absorb, so curtailment increases. For developers, this situation does not necessarily constitute waste; the additional capacity can serve as a reserve for future expansion or productive uses, provided there is a realistic expectation of demand growth or the implementation of load-shifting strategies. Additionally, considering the lifetime operation, the minimum diesel share of the optimal solutions is still not zero, due to the rainy season in July and August.
4. **Demand-growth sensitivity is strongly location-dependent and correlates with baseline diesel reliance.** In scenarios where demand increases by 20%, the additional fuel costs are substantial for smaller systems already operating near the limits of their generators, whereas larger or more balanced systems experience a much smaller marginal fuel penalty. This observation indicates that the benefits of sizing systems to be robust to demand growth depend heavily on the likelihood of future demand increases and on the site's capacity to accommodate new productive loads.

https://doi.org/10.3390/su18147263

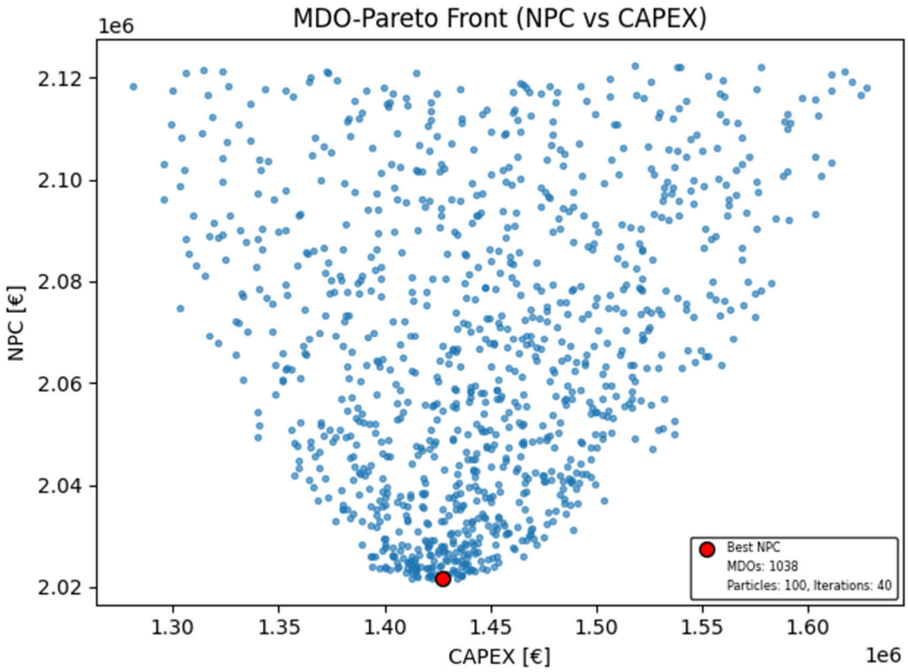

Figure 11. MDO-Pareto front showing the NPC vs. CAPEX trade-off across near-optimal designs. The asymmetric penalty of undersizing is clearly visible. The dots indicate solutions explored by the PSO.

7. Conclusions

This study demonstrates the value of the PSO-MDO framework for sustainable microgrid sizing in off-grid contexts. The key findings confirm that purely economic optimization (NPC minimization) provides an incomplete picture of system performance, and that use-case-oriented post-processing of the near-optimal region can reveal critical trade-offs between cost, resilience, and component longevity that a single NPC ranking does not expose.

Future Research Directions

1. Deep analysis of model resilience for future scenario exploration (i.e., several types of load growth patterns).
2. Implementation of advanced cost function, including other factors besides NPC, such as resilience and battery health.
3. Deep analysis of long-term Areza data to improve understanding of load profiles, plant component resilience and breakpoints, and to improve model realism and robustness.
4. Systematic sensitivity analysis of the economic assumptions—in particular, diesel price, discount rate, PV and BESS CAPEX, and the ENS penalty—to quantify the width and center of the near-optimal region and confirm the robustness of the design recommendations.
5. Potential use and comparison of different ML/AI algorithms to develop a toolbox with multiple choices for different use cases.

Author Contributions: Conceptualization, M.S., M.B. and S.H.; Methodology, A.M., A.A., M.S. and S.H.; Software, A.A., M.S. and M.B.; Validation, A.M., A.A., M.S. and M.B.; Investigation, A.A.; Data curation, A.A., M.S., M.B., S.B. and S.H.; Writing–original draft, A.M. and M.S.; Writing–review & editing, A.A. and S.B.; Visualization, M.B. and S.B.; Supervision, A.M. All authors have read and agreed to the published version of the manuscript.

Funding: This research received no external funding.

Institutional Review Board Statement: Not applicable.

Informed Consent Statement: Not applicable.

Data Availability Statement: A sample of the raw data supporting the conclusions of this article will be made available by the authors on request.

Conflicts of Interest: The authors declare no conflict of interest.

References

1. Birkl, P.R.; Roberts, M.R.; McTurk, E.; Bruce, P.G.; Howey, D.A. Degradation Diagnostics for Lithium Ion Cells. *J. Power Sources* **2017**, *341*, 373–386. [CrossRef]
2. Cicilio, P.; Orosz, M.; Mueller, A.; Cotilla-Sanchez, E. uGrid: Reliable Minigrid Design and Planning Toolset for Rural Electrification. *IEEE Access* **2019**, *7*, 163988–163999. [CrossRef]
3. International Energy Agency. *Batteries and Secure Energy Transitions*; IEA Publications: Paris, France, 2023. Available online: https://www.iea.org/reports/batteries-and-secure-energy-transitions (accessed on 30 June 2026).
4. International Energy Agency (IEA); International Renewable Energy Agency (IRENA); United Nations Statistics Division (UNSD); World Bank; World Health Organization (WHO). *Tracking SDG 7: The Energy Progress Report 2025*; International Energy Agency; Custodian Agencies: Paris, France, 2025. Available online: https://www.iea.org/reports/tracking-sdg7-the-energy-progress-report-2025 (accessed on 30 June 2026).
5. Energy Sector Management Assistance Program (ESMAP). *Mini Grids for Half a Billion People: Market Outlook and Handbook for Decision-Makers*; World Bank: Washington, DC, USA, 2022. Available online: https://documents1.worldbank.org/curated/en/099635009232259510/pdf/P1751510dd4ab407e083a6098d1905fa94f.pdf (accessed on 30 June 2026).
6. European External Action Service (EEAS). *Solar PV Mini Grids for Two Rural Towns of Areza and Maidma and Surrounding Villages in Eritrea*; European External Action Service (EEAS): Brussels, Belgium, 2014.
7. Fioriti, D.; Lutzemberger, G.; Poli, D.; Duenas-Martinez, P.; Micangeli, A. Heuristic Approaches to Size Microgrids: A Methodology to Compile Multiple Design Options. In Proceedings of the 2020 IEEE International Conference on Environment and Electrical Engineering and 2020 IEEE Industrial and Commercial Power Systems Europe (EEEIC/I&CPS Europe), Madrid, Spain, 9–12 June 2020; pp. 1–6. [CrossRef]
8. Fioriti, D.; Poli, D.; Duenas-Martinez, P.; Micangeli, A. Multiple Design Options for Sizing Off-Grid Microgrids: A Novel Single-Objective Approach to Support Multi-Criteria Decision Making. *Sustain. Energy Grids Netw.* **2022**, *30*, 100644. [CrossRef]
9. Gelchu, M.A.; Ehnberg, J.; Shiferaw, D.; Ahlgren, E.O. Impact of Demand-Side Management on the Sizing of Autonomous Solar PV-Based Mini-Grids. *Energy* **2023**, *278*, 127884. [CrossRef]
10. Ghebrezgabher, M. Estimating Solar Energy Potential in Eritrea: A GIS-Based Approach. *J. Fundam. Renew. Energy Appl.* **2022**, *3*, 155–164.
11. *Global Solar Atlas 2.0*; Solargis s.r.o. on Behalf of the World Bank Group: Washington, DC, USA, 2019. Available online: https://globalsolaratlas.info (accessed on 19 June 2026).
12. NASA POWER. *Prediction of Worldwide Energy Resources*; NASA Langley Research Center: Hampton, VA, USA, 2025. Available online: https://power.larc.nasa.gov (accessed on 19 June 2026).
13. HOMER Energy. Levelized Cost of Energy (LCOE). Available online: https://www.homerenergy.com/products/pro/docs/3.15/levelized_cost_of_energy.html (accessed on 19 January 2026).
14. Miranda, L.J.V. PySwarms: A Research Toolkit for Particle Swarm Optimization in Python. *J. Open Source Softw.* **2018**, *3*, 433. [CrossRef]
15. Perez, R.; Ineichen, P.; Seals, R.; Michalsky, J.; Stewart, R. Modeling Daylight Availability and Irradiance Components from Direct and Global Irradiance. *Sol. Energy* **1990**, *44*, 271–289. [CrossRef]
16. Maxwell, E.L. *A Quasi-Physical Model for Converting Hourly Global Horizontal to Direct Normal Insolation*; Solar Energy Research Institute: Golden, CO, USA, 1987.
17. Severson, K.A.; Attia, P.M.; Jin, N.; Perkins, N.; Jiang, B.; Yang, Z.; Chen, M.H.; Aykol, M.; Herring, P.K.; Fraggedakis, D.; et al. Data-driven prediction of battery cycle life before capacity degradation. *Nat. Energy* **2019**, *4*, 383–391. [CrossRef]